

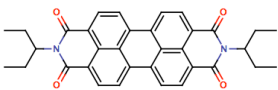
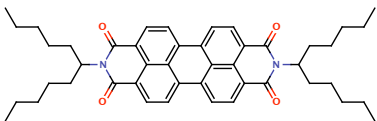
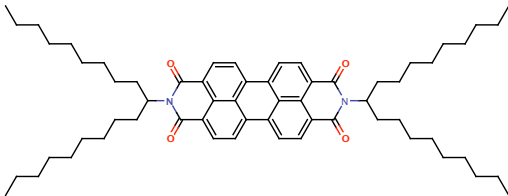
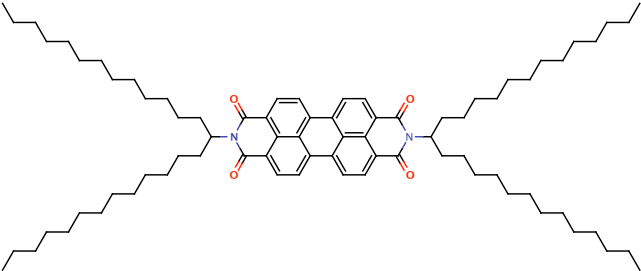
Electronic Supplementary Information

The effects of donor:acceptor intermolecular mixing and acceptor crystallization on the composition ratio of blended, spin coated organic thin films

*Matthew T. Weintraub, Enia Xhakaj, Ashli Austin, and Jodi M. Szarko**

1. Fabrication of the perylene diimide derivatives.

The molecules studied in this work are shown in Scheme S1. The reference names are also given.

Name	Structure	Abbreviation
<i>N,N'</i> -Bis(3-pentyl)perylene-3,4,9,10-bis(dicarboximide)		B2
<i>N,N'</i> -Bis(6-undecanyl)perylene-3,4,9,10-bis(dicarboximide)		B5
<i>N,N'</i> -Bis(10-nondecanyl)perylene-3,4,9,10-bis(dicarboximide)		B9
<i>N,N'</i> -Bis(14-heptacosanyl)perylene-3,4,9,10-bis(dicarboximide)		B13

Scheme S1. The names and structures of the PDI molecules used in this investigation.

B2 was purchased from Aldrich. B5, B9, and B13 were synthesized in our lab. The perylene-tetracarboxylic dianhydride (PTCDA) used in these syntheses was also purchased from Aldrich.

General Experimental Procedures. The synthesis of B5 and B9 were performed using methods that were fabricated using previous methods.¹⁻⁴ In order to maintain an excess of PTCDA, 3.7 mmol of PTCDA and 9.4 mmol of the corresponding amine were combined in 6g of imidazole solvent and stirred for 3 hours at 140°C. Upon cooling, 100mL of ethanol was used to disperse the formed product and 250mL of 2M HCl was added to the mixture, resulting in a dark, faintly purple mixture which was then stirred overnight. All substances were dried at 80°C or 100°C. The ¹H and ¹³C NMR were recorded at 400 MHz and 100 MHz, respectively. All chemical shifts in the ¹H NMR are reported in ppm relative to TMS (δ =0.00 ppm) and in the ¹³C NMR are reported in ppm relative to CDCl₃ (δ =77.16 ppm). The ¹H NMR results for all PDI molecules and the ¹³C NMR results for B13 are shown at the end of this section in **Fig. S1**. Flash chromatography was performed on 60 Å silica gel (40-75 mm). Anhydrous diethyl ether and toluene were used without further purification.

Synthesis of *N,N'*-bis(1-hexylpentyl)peryene-3,4,9,10-tetracarboxylic diimide (B5). The literature procedure² gave B5 as a crystalline, red solid: mp 179-180°C (lit. mp 183-184 °C).³ ¹H NMR (400 MHz, CDCl₃) δ 8.73-8.63 (m, 8H), 5.19 (m, 2H), 2.25 (m, 4H), 1.87 (m, 4H), 1.39-1.15 (m, 24H), 0.83 (t, J = 7.1 Hz, 12H).

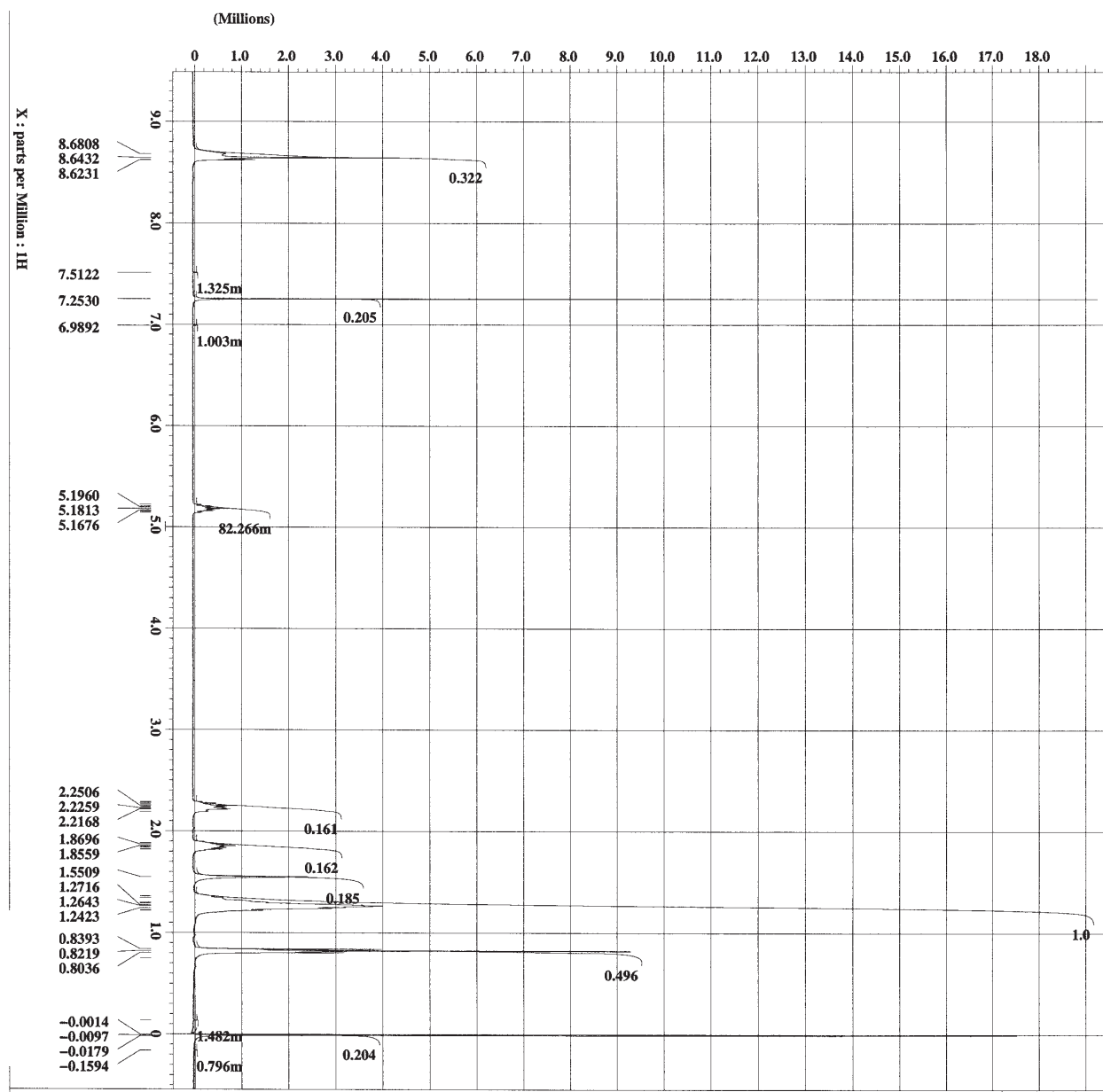
Synthesis of *N,N'*-bis(1-nonyldecyl)peryene-3,4,9,10-tetracarboxylic diimide (B9). The literature procedure for the synthesis of B5^{1,2} was modified (using 10-aminononadecane instead of 6-aminoundecane) to give B9 as a crystalline, red solid: mp 89-91°C (lit. mp 97-99 °C).⁴ ¹H NMR

(400 MHz, CDCl₃) δ 8.73-8.63 (m, 8H), 5.18 (m, 2H), 2.25 (m, 4H), 1.85 (m, 4H), 1.39-1.13 (m, 56H), 0.82 (t, J = 7.0 Hz, 12H).

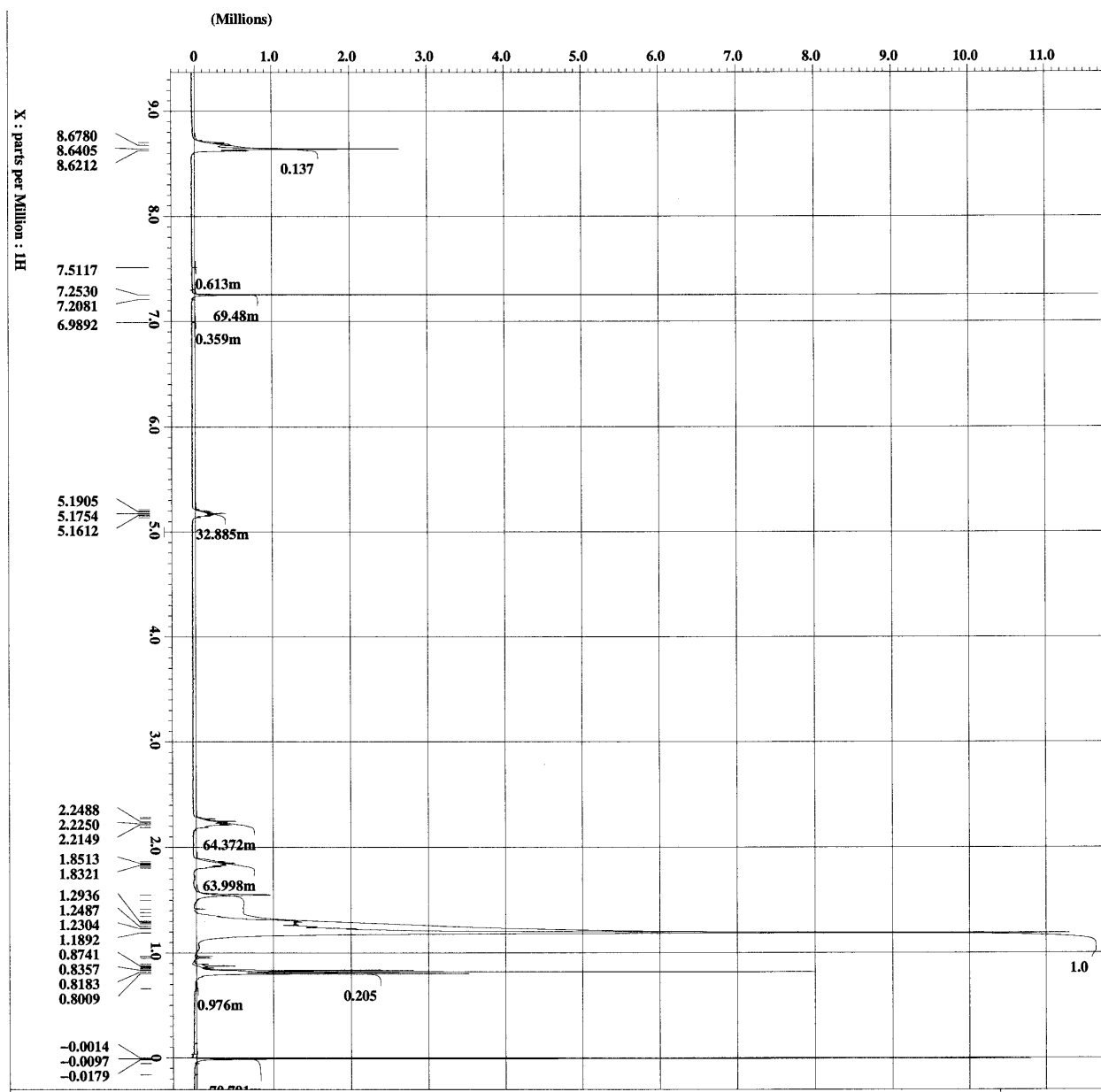
Synthesis of *N,N'*-bis(1-tridecyltetradecyl)perylene-3,4,9,10-tetracarboxylic diimide (B13). The literature procedures described for the synthesis of 10-aminononadecane⁴ and B5² were modified to synthesize 14-aminoheptacosane and B13, respectively. To a solution of 14-heptacosanone (3.50 g, 8.87 mmol) in EtOH (25 mL) and pyridine (5 mL) was added hydroxylamine hydrochloride (1.25 g, 18.0 mmol). The reaction mixture was refluxed for 20 h, cooled, transferred to a separatory funnel with hexanes (100 mL), washed with brine, and the volatiles were removed on the rotary evaporator to give the crude 14-heptacosanone oxime (3.14 g) as a solid. The crude oxime was dissolved in toluene (50 mL) and Red-Al (10 mL, 60% in toluene, 30.7 mmol) was added over 20 min with cooling by a water bath and then refluxed for 2 h. The reaction mixture was carefully quenched with 5% HCl (50 mL) and 12M HCl (10 mL) and stirred at 22 °C for 18 h. After transferring to a separatory funnel with hexanes (50 mL), the organic phase was separated and washed with brine (100 mL), dried over Na₂SO₄, and the volatiles were removed on the rotary evaporator to give the crude amine (3.0 g) as a white solid. Flash chromatography (silica gel; hexanes→50% EtOAc in hexanes) gave the 14-aminoheptacosane (1.25 g) as a white solid contaminated with 14-heptacosanone (5% by weight). A mixture of 14-aminoheptacosane (1.12 g, 2.83 mmol), perylene-3,4,9,10-tetracarboxylic dianhydride (0.40 g, 1.02 mmol), and imidazole (1.60 g, 23.5 mmol) were heated to 180 °C for 4 h under Ar. After cooling, the reaction mixture was taken up in toluene (40 mL) and 2 M HCl (30 mL) and stirred for 16 h at ambient temperature. The mixture was transferred to a separatory funnel with hexanes (100 mL), the organic phase was separated, dried over Na₂SO₄,

and the volatiles were removed on the rotary evaporator. Flash chromatography (hexanes→50% CH₂Cl₂/hexanes) gave B13 (1.01 g, 86% yield based on perylene-3,4,9,10-tetracarboxylic dianhydride) as a red wax: mp 84-86 °C. ¹H NMR (400 MHz, CDCl₃) δ 8.68-8.54 (m, 8H), 5.19 (m, 2H), 2.26 (m, 4H), 1.87 (m, 4H), 1.39-1.15 (m, 88H), 0.85 (t, *J* = 6.8 Hz, 12H); ¹³C NMR (100 MHz, CDCl₃) δ 164.7, 163.7, 134.5, 132.0, 131.2, 129.7, 126.5, 124.0, 123.3, 123.1, 54.9, 32.5, 32.0, 29.80, 29.76, 29.72, 29.68, 29.5, 27.1, 22.8, 14.2. Found: C, 81.79; H, 10.51. C₇₈H₁₁₈N₂O₄ requires C, 81.62; H, 10.36

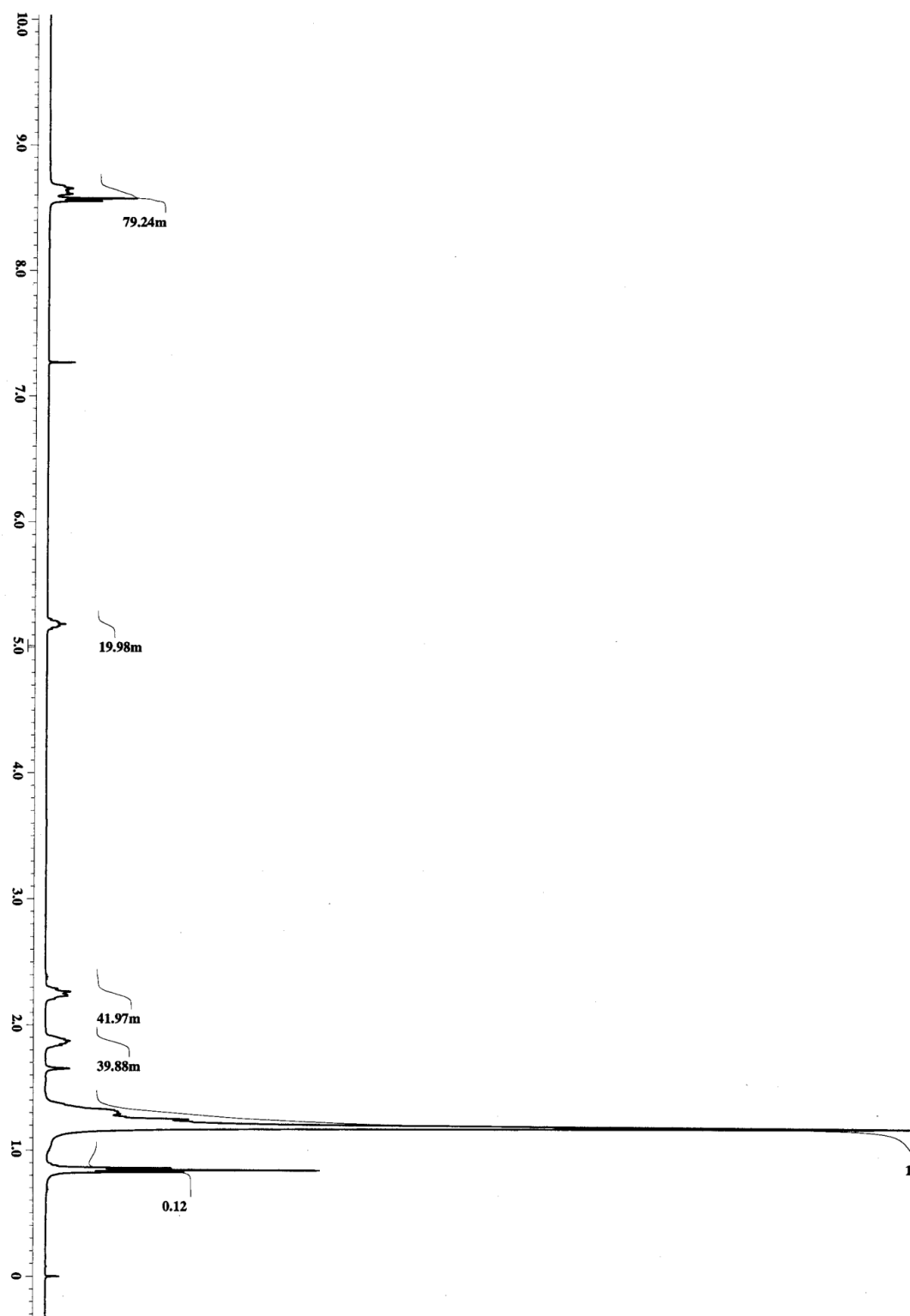
a)



b)



c)



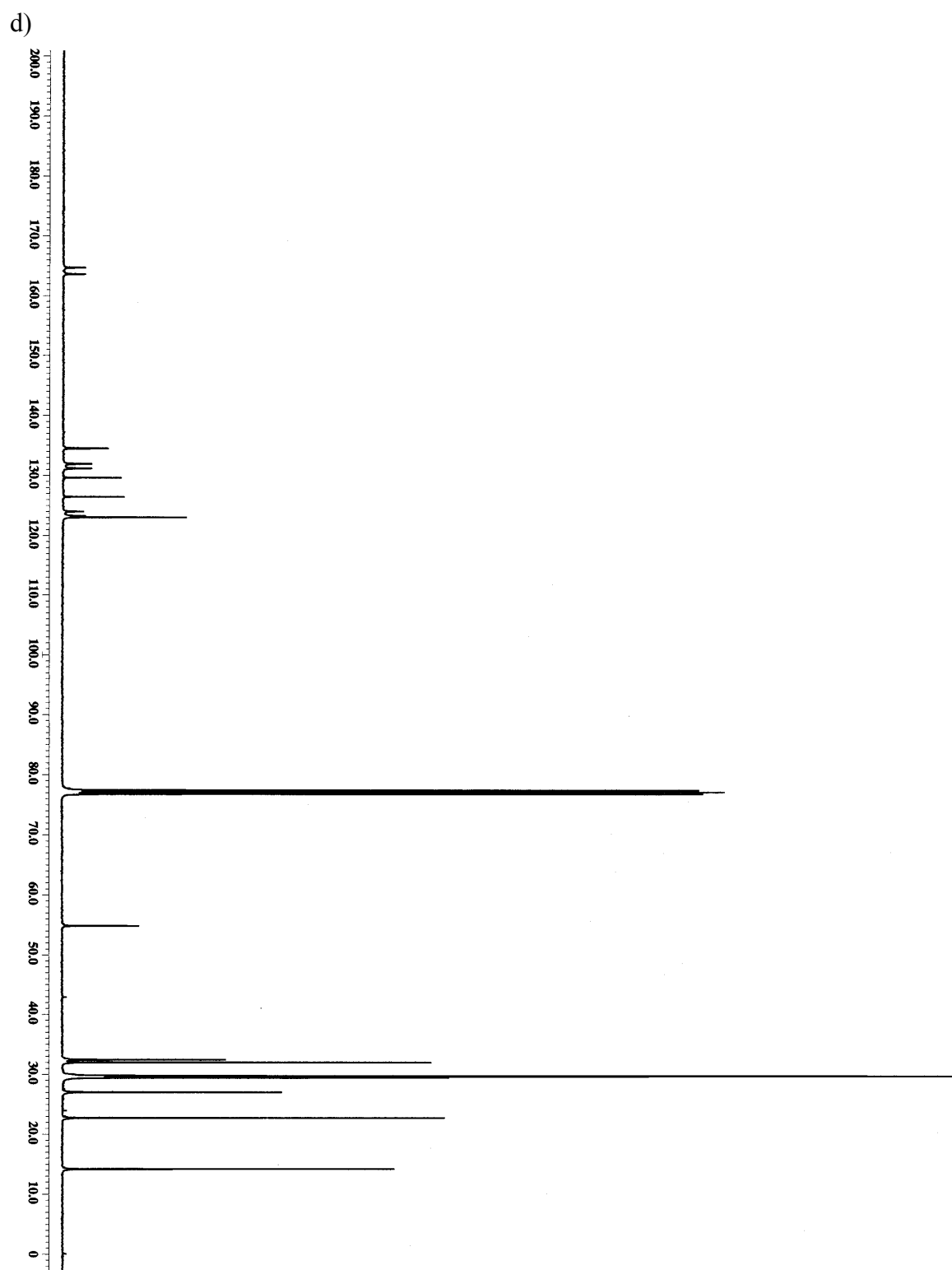


Fig. S1. The ^1H NMR spectra of a) B5 b) B9 c) B13 and d) the ^{13}C NMR spectrum of B13

2. Spectroscopic data

The spectral analysis of the blended films used in this investigation is shown in **Fig. S2**. The normalized absorption spectra of the reconstituted films are shown to better compare the change in the shapes of the spectra for each film. The reconstituted film spectra, which are shown as the solid grey lines, are compared to their casting solutions, which are shown as the solid purple lines. The dotted lines represent the fits of these spectra.

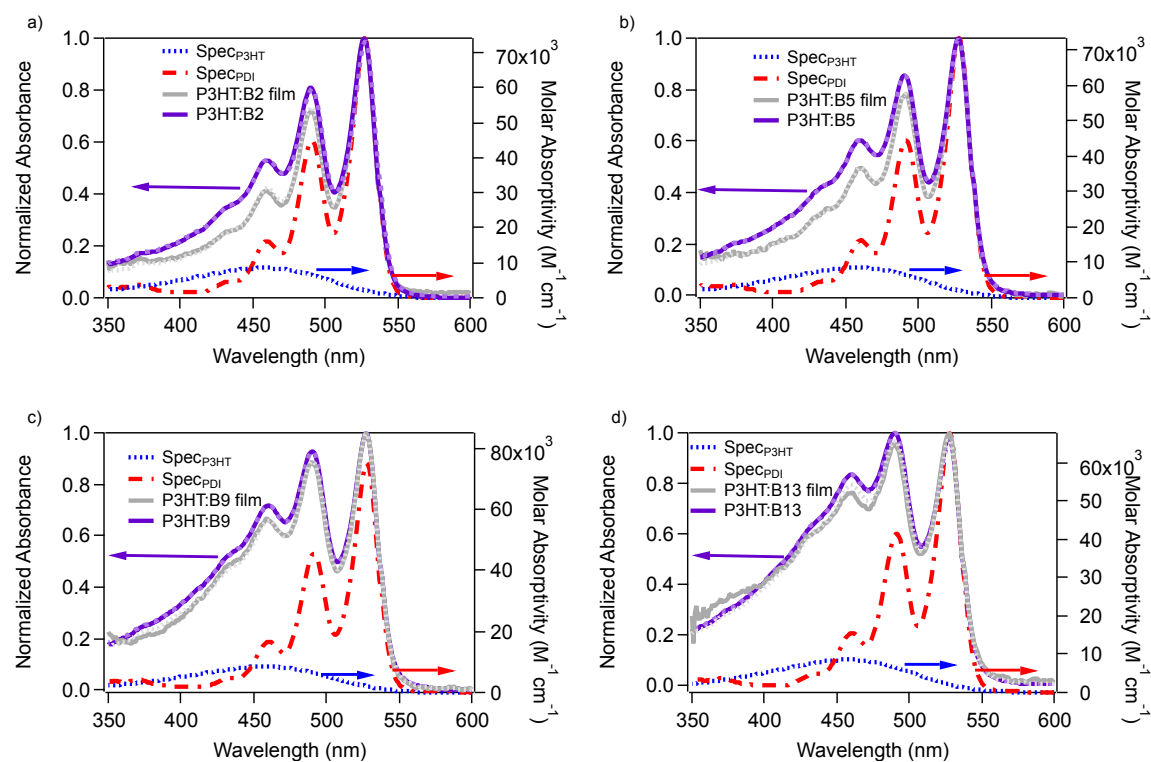


Fig. S2. Spectral comparisons of blended films of a) B2:P3HT b) B5:P3HT c) B9:P3HT d) B13:P3HT compared to the casting solutions from which they were made.

3. Optical Images of pristine PDI films

The optical images of spin cast B2, B5, B9, and B13 are shown in **Fig. S3**. B2 shows the presence of microcrystallites while B9 and B13 indicate amorphous aggregation on the micron scale. The B6 films were fairly uniform with small pockets of crystal formation.

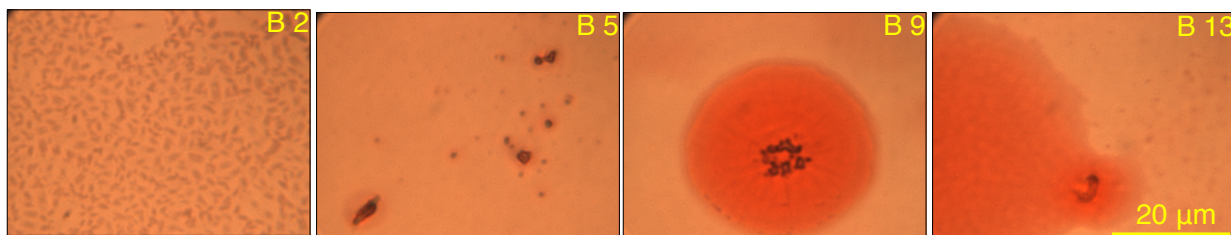


Fig. S3. Optical images of pristine PDI films investigated in this work. The scale bar indicated on the B13 image is accurate for all images presented here.

4. AFM P3HT images and line profiles

AFM images were used to estimate the film thickness and surface roughness of the pristine and blended films studied in this work. Line profiles of pristine B2 and P3HT films are shown in **Fig. S4**. The average height in the AFM images is 27.5 nm for B2. The RMS height is 29.7 nm. The average height for the P3HT images was 3 nm. The P3HT film is more amorphous than B2. Therefore, the surface roughness is lower for P3HT. The surface roughness in B2 is attributed to the presence of microcrystallites, which is the dominate phase in B2. Therefore, the crystal heights are a direct measure of the average film thickness in the B2 samples. In contrast, this method is not ideal in determining the film thickness for P3HT.

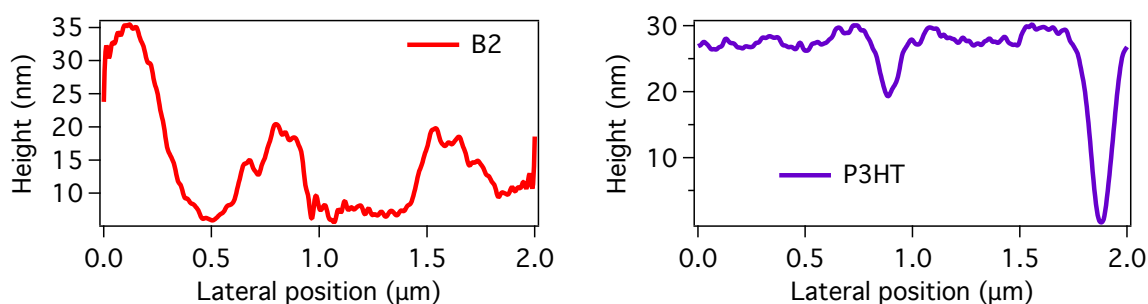


Fig. S4. AFM line profiles of a) B2 and b) P3HT

For comparison to the PDI images shown in the main body of this work, the AFM image of P3HT is also shown here in **Fig. S5**.

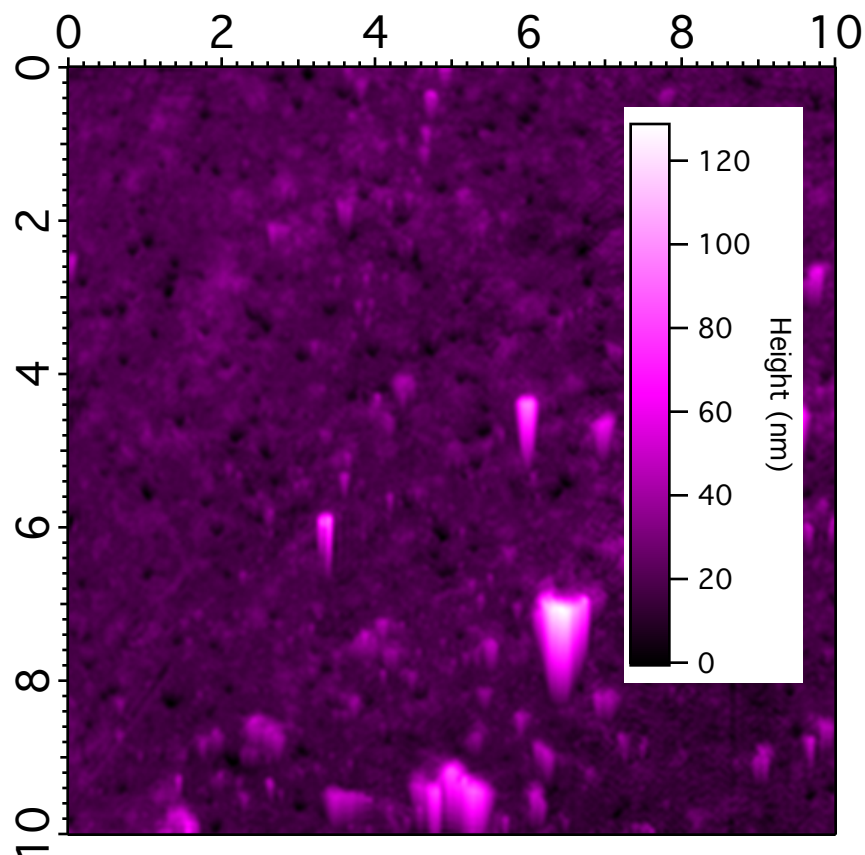


Fig. S5. Typical AFM image of a pristine P3HT film (10 μm x 10 μm). Small valleys in the film are observed along with aggregated areas of P3HT.

5. Estimating the film thicknesses of pristine P3HT and PDI films spectroscopically.

The thickness of the B5 pristine films as a function of spin speed is shown in **Fig. S6**. The casting solution concentrations were kept constant for this investigation, so the film thickness depends on the spin speed by the relationship $d = A \cdot \omega^{-1/2}$, where d is the film thickness, A is the amplitude, which is dependent on the solvent viscosity and solution concentration, and ω is the spin speed in rpm.⁵⁻⁷ The relationship holds well for the B5 film. The quality of the films as a function of spin speed was also monitored by optical microscopy. For all spin speeds, the films were of high quality, but the uniformity was slightly degraded at spin speeds below 1000 rpm.

Therefore, spin speeds of 1000 rpm were used to determine the dependence of molecular variation on BHJ blend ratios, which is the main focus of this investigation.

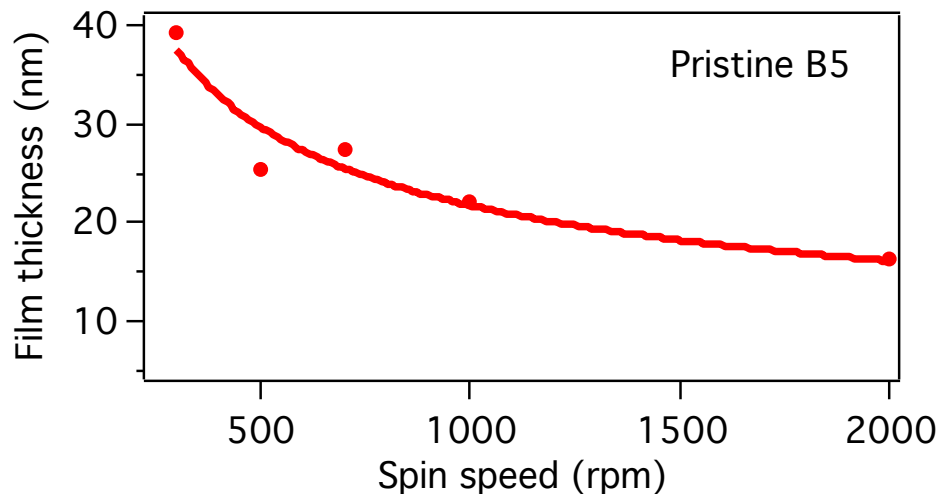


Fig. S6. Spin speed dependence on the film thickness of B5.

Quantifying the film thickness of blended films presents a number of challenges. The films have a mixture of crystalline and amorphous sites for many of the systems, so typical techniques such as ellipsometry can be difficult to interpret. To estimate our film thicknesses, we used a combination of AFM line profiles and spectral modeling. The film thickness of B5 was determined using the following method. The concentrations of the reconstituted solutions were used to estimate the thickness of our pristine films. The area of the films used for the reconstituted solutions was 1.25 cm². The volume of our films was 1.5 mL. The film thickness can therefore be estimated using the following relationship:

$$a(nm) = \frac{M \cdot V \cdot MW}{d \cdot A} \cdot 10^7$$

where M is the concentration of the reconstituted film, V is the volume of the solution, MW is the molar mass of the molecule (698.9 g/mol), d is the predicted density of B5, A is the area of the film reconstituted into solution, and the scaling factor is needed to convert from cm to nm. The predicted density of this molecule was found using SciFinder Scholar.⁵ The calculation above is compared to the line profiles obtained using AFM, which is shown in **Fig. S7**.

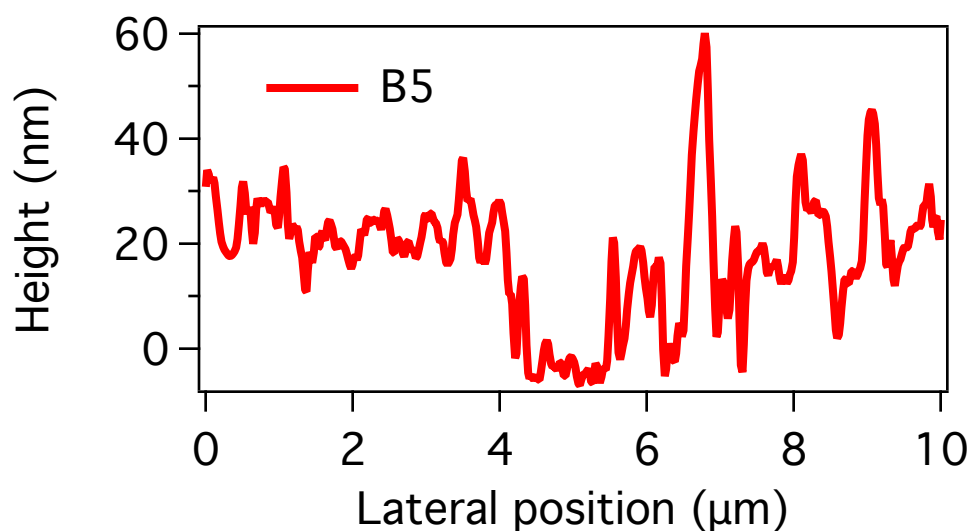


Fig. S7. AFM line profile for B5

The average height of the B5 film is 19.9 nm in AFM. This corresponds very well with the estimated results calculated above. The semicrystalline state of B5 assures good agreement of the thickness using AFM measurements and the density calculations described above.

To further verify the use of density calculations to estimate our film thicknesses, the crystallographic data for B2 was used to estimate the density of B2. The unit cell has 8 monomer units and an area of 5330.34 Å³. The molar mass of the molecule is 530.61 g/mol. Therefore, the density of the molecule can be calculated using the following equation:

$$density(\frac{g}{cm^3}) = \frac{Z \cdot MW}{area(cm^3) \cdot N_A}$$

Where Z is the number of molecules in a unit cell, $area$ is the unit cell area, MW is the molar mass of the molecule, and N_A is Avagadro's number. This result yields a density of 1.32 g/cm^3 , which is very close to the predicted density of 1.35 g/cm^3 . The combination of these density calculations gives us continuity in our density calculations. The B2 appears to be mainly crystalline in form while P3HT has a more complicated composition of crystalline and amorphous states. Therefore, the reported density of 1.1 g/cm^3 was used to calculate the thickness of P3HT. Using the density of 1.32 g/cm^3 and 1.1 g/cm^3 for B2 and P3HT, respectively, the thickness for the B2 films was $21.9 \pm 0.5 \text{ nm}$ while the thickness for the P3HT was $30. \pm 3 \text{ nm}$. Using predicted densities for B5, B9, and B13, the estimated films thicknesses were $26 \pm 1 \text{ nm}$, $25.3 \pm 0.5 \text{ nm}$, and $25 \pm 1 \text{ nm}$, respectively.

6. Solubility check and concentration dependence for the B2 and P3HT:B2 parent solutions.

The concentration of the parent solutions in this work are below the solubility threshold for our molecules studied. If aggregates are forming and crashing out of solution, then this would affect the composition results of our experiment. Therefore, we have verified that the parent solution is not changing its composition ratio due to solubility effects. To do this, we measured the absorption spectrum of the solutions before and after using a $0.2 \text{ }\mu\text{m}$ PTFE filter to get rid of any aggregates in the solution. The B2 molecule is the least soluble, so we used this as our test molecule. The solutions were heated to 60° C and then cooled to room temperature. We did this

for B2, P3HT, and blended solutions. After filtration, both the filtered and unfiltered solutions were diluted by 400 times to accurately record the absorbance spectrum of our solutions. The spectra recorded are shown in **Fig. S8**. We observed no change in the intensity of the absorption spectrum upon doing this. We also did not observe any appreciable redshift in the absorption spectrum, which would indicate aggregation. Finally, the predicted absorbance of our spectra was 2.1, and our measured absorbance was 2.2. This is within the standard error for our experiments, so we can conclude that the sample is dissolved completely.

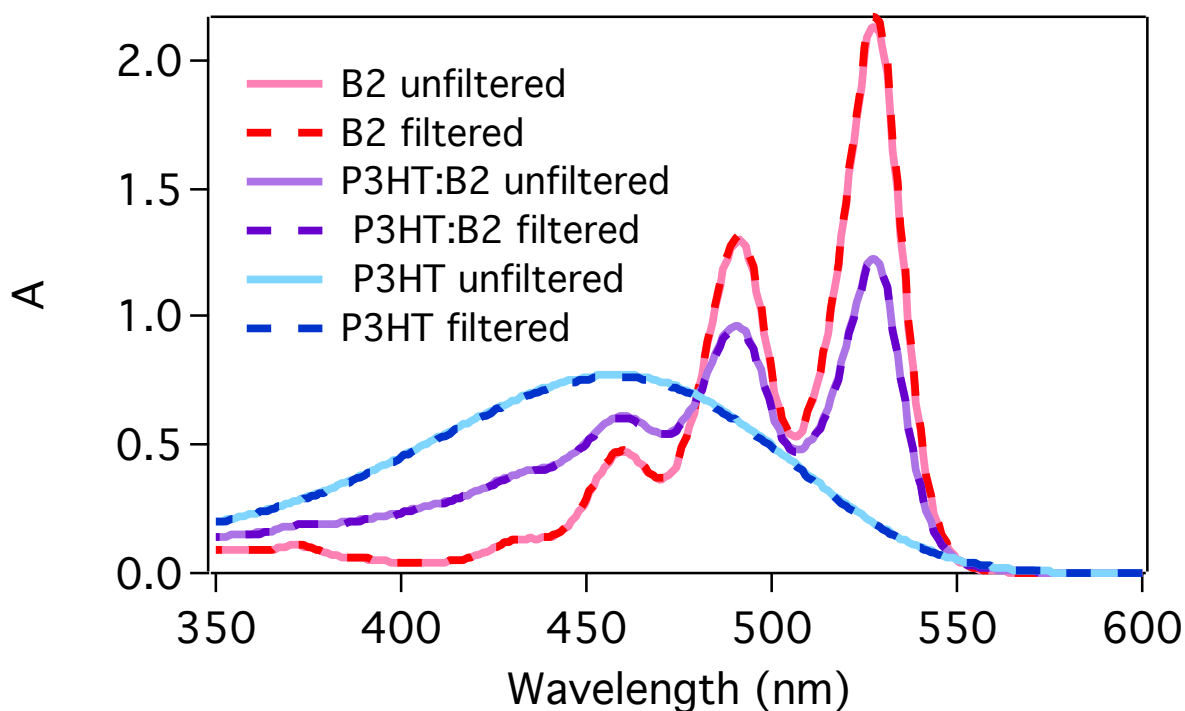


Fig. S8. Solution absorption spectra of the films used to make the P3HT:B2 films investigated in this work.

We also performed absorbance measurements using a 0.1 mm cuvette for the undiluted casting solutions. Even with such a short path length, the absorbance is too high to measure at the peak

wavelengths. Nevertheless, this data is meaningful. We still do not observe any peaks in the 550-600 nm region for B2 or P3HT, which typically indicates aggregation. Lowering the temperature of the solutions also did not facilitate aggregation, so the solutions are well within the range of solubility. These spectra are shown in **Fig. S9**. Therefore, we can conclude that B2 is soluble at this concentration. The other molecules are more soluble than B2, so we can safely assume that all molecules are soluble at 6 mg/mL.

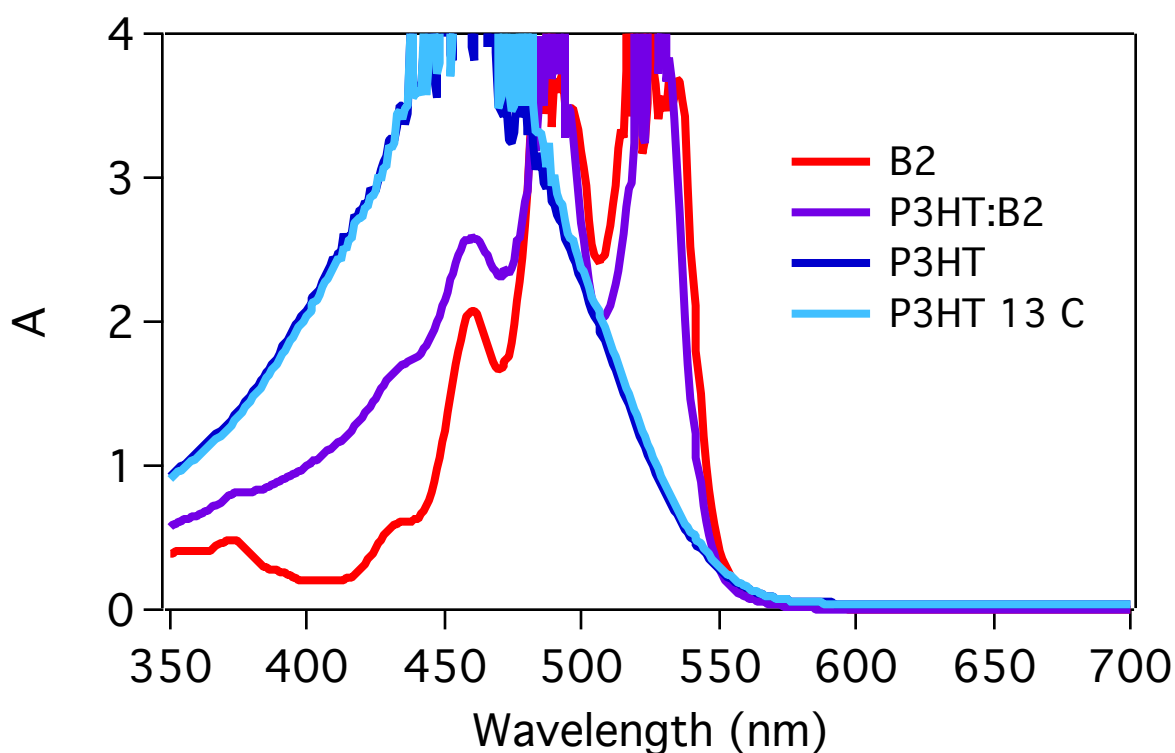


Fig. S9. Absorption spectra of the casting solutions at full concentration using 0.1 mm cuvettes. All other diluted spectra were taken using 1 cm cuvettes. The P3HT solution was taken at room temperature and 13° C.

The concentration of the casting solution will also affect the morphology and composition ratio of the films. A rough comparison of a P3HT:B2 film fabricated using a 30 mg/mL casting

solution was performed. The optical images of a) a P3HT:B2 film made from a 6 mg/mL casting solution and b) a P3HT:B2 film made from a 30 mg/mL casting solution are shown in **Fig. S10**. The films made from the higher concentration solution clearly shows large aggregates in the micron range. The spectral analysis for the high concentration film is shown in **Fig. S11**. These preliminary results show that the amount of P3HT is slightly enhanced compared to the B2 concentration in these films. The change in composition ratio is attributed to the aggregation of B2 in the solution prior to film casting. The casting solution in which the film was prepared also had a higher initial P3HT concentration, indicating the depletion of B2 from the solution at early times.

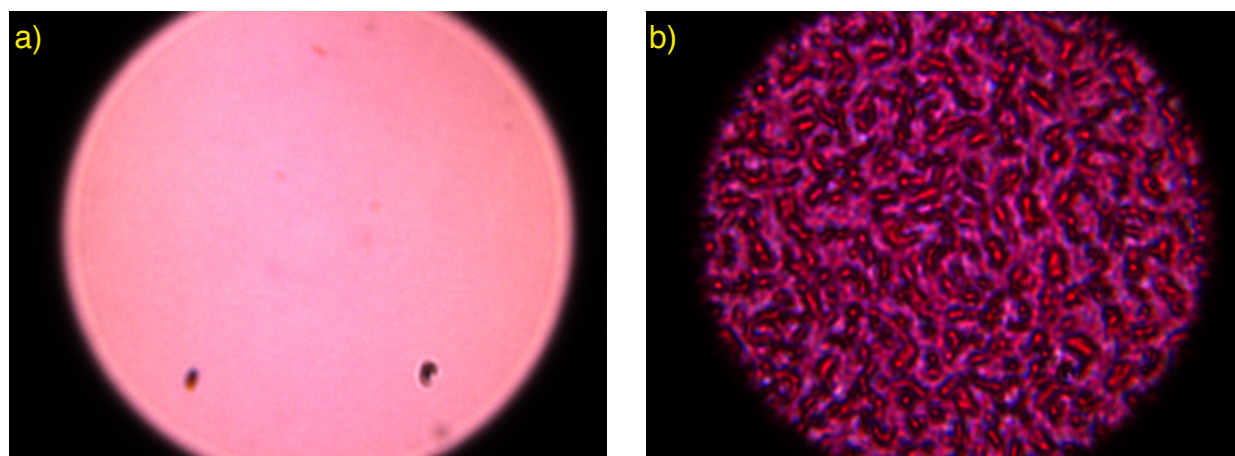


Fig. S10. Optical microscope images of P3HT:B2 films made from a) 6 mg/mL and b) 30 mg/mL casting solutions.

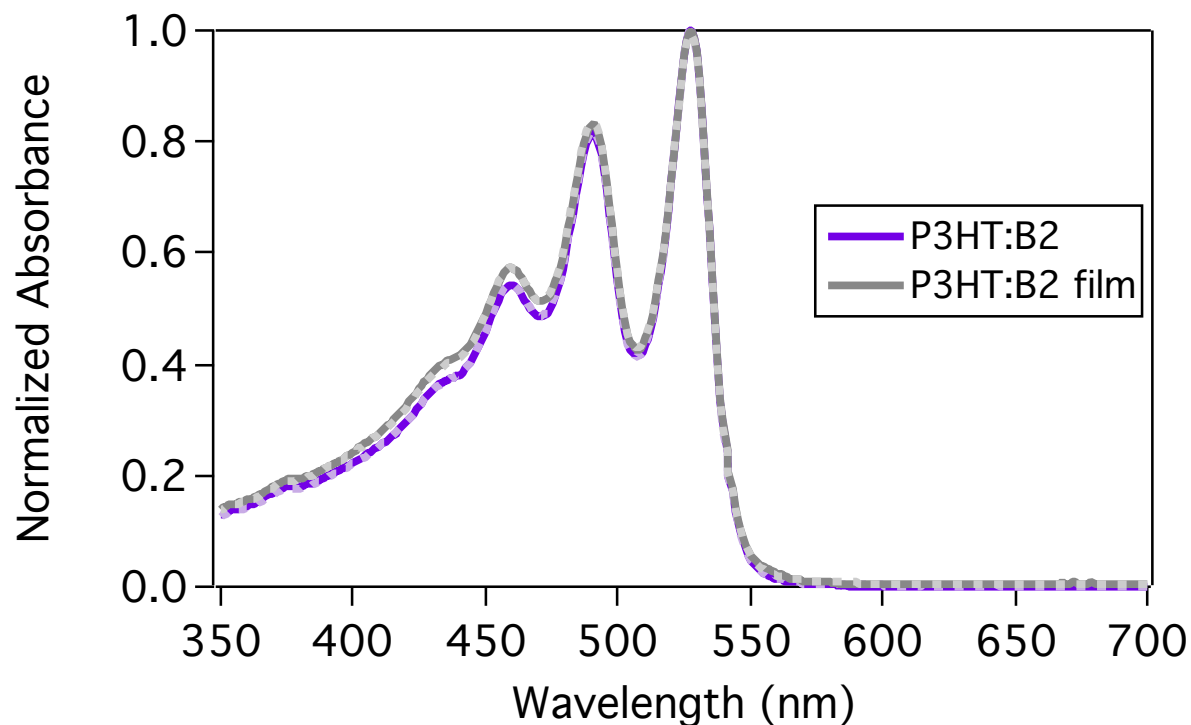


Fig. S11. Spectral analysis of the film cast from the 30 mg/mL solution. The purple curve is the spectrum of the casting solution and the grey curve is the spectrum of the reconstituted film. The solid lines are the raw data, and the dashed lines are the fit spectra.

References

- 1 K. Balakrishnan, A. Datar, T. Naddo, J. Huang, R. Oitker, M. Yen, J. Zhao and L. Zang, *J. Am. Chem. Soc.*, 2006, **128**, 7390–7398.
- 2 G. Boobalan, P. M. Imran and S. Nagarajan, *Superlattices and Microstructures*, 2012, **51**, 921–932.
- 3 S. Demmig and H. Langhals, *Chemische Berichte*, 1988.
- 4 L. D. Wescott and D. L. Mattern, *J Org Chem*, 2003, **68**, 10058–10066.
- 5 P. Yimsiri and M. R. Mackley, *Chemical Engineering Science*, 2006, **61**, 3496–3505.

- 6 E. Mohajerani, F. Farajollahi and R. Mahzoon, *J Optoelectron Adv M*, 2007.
- 7 D. W. Schubert, *Polymer Bulletin*, 1997, 177–184.